

www.acsami.org Research Article

Paper-Based Supercapacitive Pressure Sensor for Wrist Arterial **Pulse Waveform Monitoring**

Azmal Huda Chowdhury, Borzooye Jafarizadeh, Nezih Pala, and Chunlei Wang*



Cite This: ACS Appl. Mater. Interfaces 2023, 15, 53043-53052



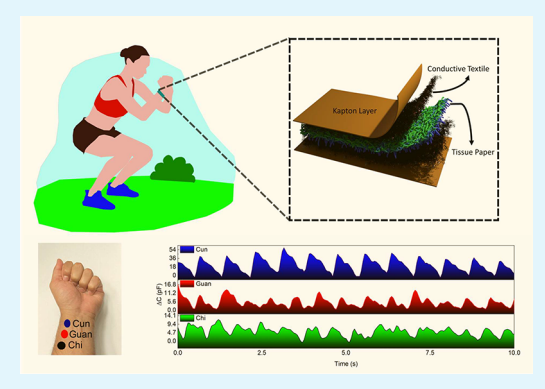
ACCESS I

Metrics & More

Article Recommendations

Supporting Information

ABSTRACT: Recent developments in wearable pressure sensors have led to the need for high sensitivity and a broad sensing range to accurately detect various physiological states. However, high sensitivity does not always translate to a wide sensing range, and manufacturing sensors with such high sensitivity is a complex and expensive process. In this study, we present a capacitive pressure sensor based on tissue paper that is simple to produce and cost-effective yet still exhibits high linear sensitivity of 2.9 kPa⁻¹ in the 0-16 kPa range. The linear sensitivity of 1.5 kPa⁻¹ was achieved from 16 to 90 kPa. The sensor also demonstrated a fast response time of 0.2 s, excellent pressure resolution at both low and high pressures, and a sufficient signal-to-noise ratio, making it ideal for detecting wrist arterial pulse waveforms. We were also able to demonstrate the sensor's practicality in real-world applications by cycling it 5000 times and showing its capability to capture pulse waveforms from different arterial



locations. These low-cost sensors possess all the intrinsic features necessary for efficient measurement of pulse waveforms, which may facilitate the diagnosis of cardiovascular diseases.

KEYWORDS: pressure sensor, electric double layer capacitor, paper-based sensing, pulse waveform monitoring

1. INTRODUCTION

Continuous improvement of the sensing mechanisms is critical for the advancement of wearable technology in this modern age. Research efforts have been focused on flexible electronics and sensors due to their bendability, conformability, and wearability features. These wearable devices provide valuable information about the physiological status of human beings, particularly targeting cardiovascular activities such as pulse waveform monitoring.¹ Maintaining cardiovascular health is crucial due to unhealthy food habits, lack of exercise, anxiety, and genetic factors leading to cardiovascular diseases (CVDs), which are the leading causes of death worldwide. According to the Centers for Disease Control (CDC), hypertension, also known as the silent killer,^{2,3} affects nearly half of adults in the United States (47%, or 116 million), and the lack of early diagnosis can result in sudden and premature death.4 The conventional method for diagnosing hypertension uses cuffbased oscillometric and auscultatory blood pressure measurements, but the bulky nature of these systems hinders continuous blood pressure measurement.²

Continuous monitoring of pulse waveforms offers an alternative to the cuff-based blood pressure monitoring system and provides valuable information about the cardiovascular system that can be used to diagnose CVD.⁵ A typical pulse waveform has three peaks, namely, the systolic peak, the diastolic peak, and the inflection peak, which hold essential information for disease prognosis. To utilize pulse waveforms

for disease diagnosis, obtaining detailed features is crucial. However, commercial wearable devices such as smartwatches use photoplethysmogram-based optical sensing (PPG), which cannot capture all intrinsic peaks from the pulse waveforms. The optical sensor often retrieves cardiovascular information from the capillaries rather than the arterial sites, leading to incomplete pulse waveform detection. Furthermore, the accuracy of PPG is affected by ambient light and skin tonality, further limiting its use in pulse waveform detection.

Flexible pressure sensors have emerged as a promising tool for physiological monitoring, particularly in capturing pulse waveforms from arterial sites. This is due to their ability to capture tiny deformations caused by arterial blood flow and translate them into pulse waveforms. Unlike PPG-based sensors, flexible pressure sensors are not limited by skin tonality issues or ambient conditions, making them suitable for the continuous monitoring of pulse waveforms. However, to effectively capture all the details of the pulse waveforms, flexible pressure sensors must have high sensitivity, a fast response time, a broad pressure sensing range, and a high

June 19, 2023 Received: Revised: August 24, 2023 Accepted: October 5, 2023 Published: November 3, 2023





signal-to-noise ratio (SNR).^{1,8} There are different types of sensing mechanisms, including capacitive, piezoresistive, piezoelectric, and triboelectric sensing, each with their own advantages and disadvantages.^{9–11} Among these, capacitive sensors have emerged as a promising option due to their simple working mechanism, low power requirement, and less dependence on environmental issues.^{11–18} These lightweight and portable sensors can be powered by lithium-ion batteries or supercapacitors for wearable applications, making them an attractive option for continuous physiological monitoring.^{19,20}

Capacitive sensors employ a sensing mechanism that involves a system of parallel plate electrodes following the equation $C = \frac{\varepsilon A}{d}$, where C represents capacitance, ε represents dielectric permittivity, and A represents the surface area of the electrodes. 21,22,9,23 When pressure is applied, the electrodes and dielectric layer deform, generating a response. The pressure sensitivity of these sensors relies on the modulus of elasticity of the electrode and dielectric layer and the permittivity of the dielectric layer. However, because capacitive sensors rely on geometric changes in the sensing material, their pressure sensitivity is not typically as high as that of other sensors. 14,15 Furthermore, because their capacitance range is only in the picofarads, they are susceptible to noise interference from sources such as the body and electromagnetic waves, which can add up to more than hundreds of picofarads. ^{24–26} To address these issues, researchers have recently developed supercapacitive pressure sensors with high sensitivity and SNR as well as a long sensing range that are suitable for monitoring physiological activities. 8,15,24,25 One example of this is the iontronic sensing mechanism used by the Pan group, which utilizes a thin iontronic film to achieve electric double layer capacitance at the electrode-electrolyte interface.²⁵ With this method, they were able to achieve an ultrahigh pressure sensitivity of 3.1 nF/kPa by sandwiching a thin iontronic layer between two parallel ITO/PET electrodes. Other groups have also improved the performance of supercapacitive sensors by using microstructured ionic gels, 8,15,27 porous ionic composites, and nanofibrous ionic composites. 26,28 For example, Bai et al. developed a supercapacitive sensor with a graded intrafillable structure that achieved a high sensitivity of 3300 kPa⁻¹ with a broad pressure range of 400 kPa.²⁹ Park's group developed an electrospun nanofiber composite of MXene/ionic salt in a PVA polymermatrix-based supercapacitive sensor that achieved pressure sensitivities of 5.5 and 1.5 kPa⁻¹ in the pressure ranges of 0–30 and 30–250 kPa, respectively.²⁸ In addition, Pan et al. created a supercapacitive sensor based on a hair-like ionic hydrogel that could monitor pulse waveforms.⁸ This sensor achieved a maximum sensitivity of 2296 kPa⁻¹ in the 0-4 kPa region with a broad pressure range of 100 kPa. These supercapacitive sensors work based on an electric double layer capacitance at the electrode-electrolyte interface, which allows for a high areal capacitance that is not attainable in traditional parallel plate capacitive sensors.^{8,24} This high areal capacitance is responsible for the high baseline capacitance and capacitive signal output under pressure, resulting in a high SNR and making them less susceptible to parasitic noises.

Despite the potential of pressure sensors, their fabrication methods for achieving high performance often rely on costly or time-consuming processes. For instance, photolithographybased template fabrication methods use costly silicon wafers, while the electrospinning method requires a high voltage setting and a fine-tuning process for the desired nanofibrous membrane formation. A potential solution to this problem is the use of tissue paper as a low-cost, readily available material with a porous structure that can deform under pressure. Rather than electrospinning, a simple and cost-effective approach involves immersing tissue paper in an ionic-liquid—polymer solution to create an electrolyte layer for fabricating high-performance supercapacitive sensors.

In this study, we present the first-ever report of a tissue-paper-based supercapacitive sensor fabricated using commercially available conductive textiles as the electrode material, which further simplifies the fabrication process. The sensor's ionic properties allow it to achieve a high sensitivity of 2.9 kPa⁻¹ within the initial pressure sensing range of 0–16 kPa. Beyond 16 kPa, the sensitivity decreases to 1.5 kPa⁻¹, providing a broader detection range from 16 to 90 kPa, coupled with excellent cyclability. Due to its exceptional performance, we were able to use the pressure sensor to collect arterial pulse waveforms from various arterial locations. These low-cost, high-performance, and flexible pressure sensors can find application in point-of-care settings that demand stability, reliability, and user comfort.

2. MATERIALS AND METHODS

Materials. Orthophosphoric acid (H_3PO_4) was purchased from Sigma-Aldrich, poly(vinyl alcohol) (PVA) was purchased from Alfa Aesar, Kimtech Kimwipes were purchased from Amazon, and conductive textile was purchased from MSE supplies. All the components are available commercially and were used as supplied without any further purification.

Preparation of the PVA– H_3PO_4 Solution. First, PVA was added to deionized (DI) water in a glass beaker at a 10% weight ratio. The solution was magnetically stirred at 90 °C for 2 hours until the PVA dissolved completely. The solution was cooled to room temperature. Once the temperature had cooled down, different volumes of H_3PO_4 (85% v/v) were added to 20 mL of the PVA solution and stirred continuously for 2 hours.

Preparation of the Electrolyte Layer. First, the Kimtech wipe was placed on a cleaned plane surface. The PVA $-H_3PO_4$ solution was drop coated on the tissue paper and was uniformly spread over the surface using the blade-coating method. Multiple blade-coatings of the electrolyte were carried out to ensure the reproducibility of the process. Subsequently, the soaked tissue paper was cured inside an oven at 70 $^{\circ}C$ for 15 min.

Preparation of the Flexible Sensor. The conductive textile electrodes were cut according to desired dimensions. The electrolyte layer was cut and sandwiched between the conductive textile electrodes. The sensor was finally packaged inside commercial Kapton tape. Electrical connection was made using flexible copper tape for sensor characterization and application.

Characterization and Measurement. The morphology of the fabricated sensor was characterized by a JSM-FS100 scanning electron microscope. Fourier transform infrared spectroscopy (FTIR) was carried out using JASCO FT/IR-4100 to characterize different concentration composite samples. The sensing performance of the sensor was tested using MARK-10 ES-20 test stand connected to a MARK-10 M5-50 force gauge for precise loading. The uniform pressure was applied by a circular cap with an area of 125 mm². The capacitance of the sensors during testing and applications were measured using a precision LCR meter Agilent 4263B at a frequency of 1 kHz. The sensor data were visualized using a custom-made LABVIEW graphical user interface (GUI).

3. RESULTS AND DISCUSSION

The base material used for realizing the pressure sensor was a high-porosity, permeable Kimtech wipe that is commercially

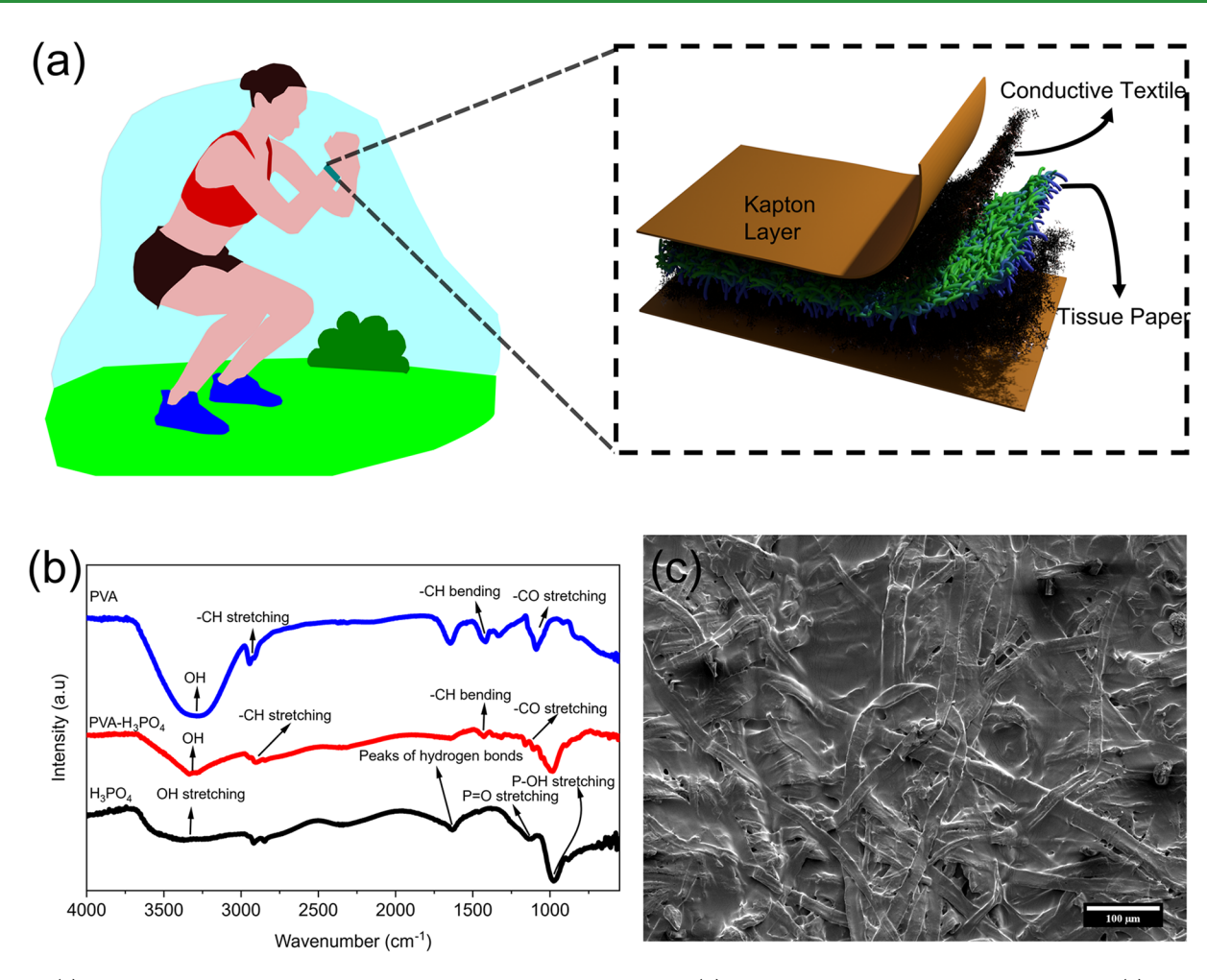


Figure 1. (a) Schematic of the tissue-paper-based supercapacitive pressure sensor. (b) FTIR spectroscopy of the electrolytic layer. (c) SEM image of the electrolytic layer.

available. These wipes are renowned for their delicate nature, superior cleaning abilities, and wide range of applications in laboratory settings. Thus, this study leveraged the unique characteristics of Kimtech wipes as the backbone for the electrolytic layer. The electrolyte layer was then created by blade-coating the PVA-based $\rm H_3PO_4$ solution on tissue paper. Due to the wipes' excellent breathability and uniform porosity, the solution quickly soaked the entire tissue paper, enabling the creation of a uniform and efficient supercapacitive pressure sensor.

Figure 1b displays FTIR characterization of the constituents of the electrolyte layer. The FTIR spectra were obtained in transmission mode within the wavenumber range of 500 to $4000~\rm cm^{-1}$. In the case of pure PVA, a large peak between 3000 and 3500 cm⁻¹ is associated with –OH stretching from the intramolecular and intermolecular hydrogen bonds. The peaks between 2750 and 3000 cm⁻¹ are linked to the C–H stretching from the alkyl group. 30,31 Additionally, the C=O and C–O stretching from the acetate group are observed between 1500 and 1750 cm⁻¹ indicative of the functional groups in the PVA polymer. The FTIR spectrum of pure $\rm H_3PO_4$ shows a broad peak between 3000 and 3500 cm⁻¹ representing the O–H stretching. A characteristic peak between 1200 and 1250 cm⁻¹ indicates P=O stretching, and a strong peak within 900–1000 cm⁻¹ could be related to P–OH stretching.

In the composite PVA-H₃PO₄, the broad peak between 3250 and 3500 cm⁻¹ is likely a result of combined O-H stretching from both PVA and H₃PO₄. The small peak between 2750 and 3000 cm⁻¹ corresponds to the C-H stretching. The peaks between 1500 and 1750 cm⁻¹ can be attributed to C=O and C-O stretching, and the strong peak around 1000 cm⁻¹, along with small peaks between 1000 and 1500 cm⁻¹, might reflect the presence of phosphoric acid groups, especially P-OH and P=O respectively. In conclusion, the FTIR characterization of the electrolyte layer unveils distinct peaks, each corresponding to different functional groups found in PVA, H₃PO₄ and the composite PVA-H₃PO₄ material.

The schematic of the sensor is presented in Figure 1a, where the electrolyte layer is positioned between two conductive textile electrodes. Additionally, the fibrous morphology of the electrolyte impregnated tissue paper is shown in Figure 1c. The tissue paper, with its porous and flexible nature, facilitates easy impregnation with the ionic liquid, a property that is further substantiated by a supplementary SEM image (Supplementary Figure S1a). The thickness of the tissue paper before electrolyte impregnation was found to be $166~\mu m$. After impregnation with PVA $-H_3PO_4$, the tissue paper's thickness changed to $267~\mu m$, as shown in the cross-sectional SEM image (Supplementary Figure S1b). Figure 1c shows tissue paper after electrolyte impregnation. EDS mapping further confirms the even coating of H_3PO_4 , as evidenced by the O-k

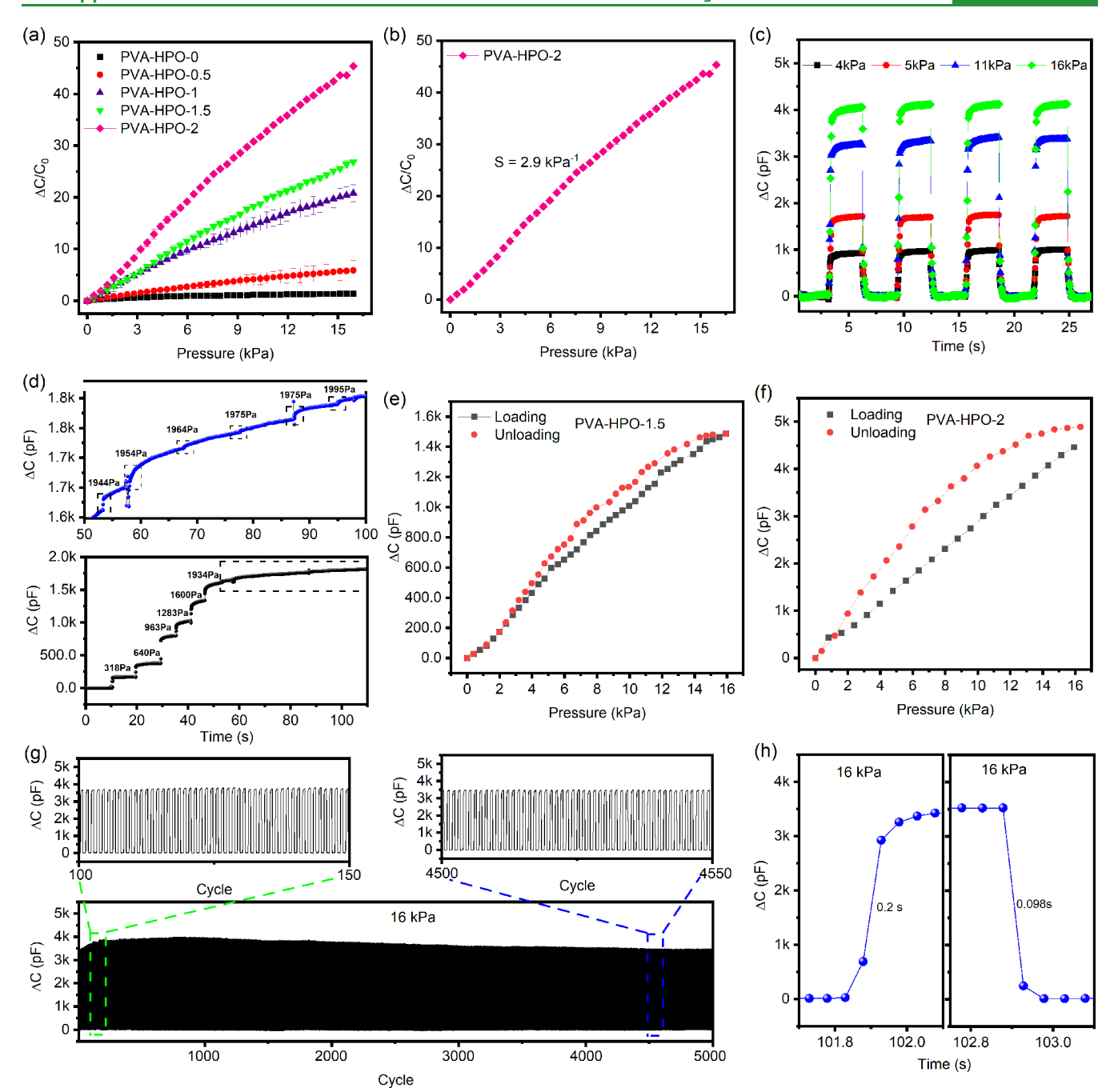


Figure 2. (a) Relative capacitance change over pressure at different electrolyte concentrations. (b) Detailed relative capacitance changes over pressure for the sensor with the highest electrolyte concentration. (c) Capacitance change over time for different pressure loadings. (d) Capacitance change over time for different low-pressure loadings. (e) Hysteresis behavior for the sensor with 1.5 mL of H₃PO₄ concentration. (f) Hysteresis behavior for the sensor with 2 mL of H₃PO₄ concentration. (g) Cyclic performance test for 5000 cycles. (h) Rise time and fall time of the sensor.

and P-k peaks (Supplementary Figure S2). Supplementary Figure S3 provides visual representation of the physical sensor highlighting the dimensions of the sensor. This combination of porosity, flexibility, and the ability to shape under pressure contributes to the unique characteristics of the sensor. Supplementary Figure S4 also illustrates the conductive textile, highlighting its soft and highly porous characteristics that contribute to the sensor's high sensitivity and large sensing range.

In Supplementary Figure S5, the sensor's sensing mechanism is depicted, indicating that without pressure the contact area between the electrodes and electrolyte layer is insufficient,

resulting in a small effective electrode to electrolyte surface area. However, when pressure is applied, the electrode—electrolyte comes into close contact, increasing the effective contact area and the accumulation of positive and negative charges at the interface. According to the parallel plate capacitance mechanism, the distance between the electrodes decreases, increasing the capacitance and producing a large change in capacitance on the order of hundreds of picofarads. This mechanism results in a higher SNR due to the formation of EDLC than traditional parallel plate capacitive sensors.

The sensitivity of a capacitive pressure sensor is defined by the equation $S = \frac{\overline{C_0}}{\Delta P}$, where ΔC refers to the change in capacitance, C_0 is the base capacitance, and ΔP denotes the applied pressure.²⁸ To achieve high sensitivity, the capacitance signal must be high, even with small pressure. The sensing performance of the fabricated pressure sensors is summarized in Figure 2. To determine the pressure sensor with the optimum pressure sensitivity, various amounts of the electrolyte were added to the PVA matrix during the fabrication of pressure sensors. In order to prepare the samples, a solution of 10 wt % PVA in DI water was first prepared. Next, different volumetric amounts of H₃PO₄ (0, 0.5, 1, 1.5, and 2 mL) were added to 20 mL of PVA solution to prepare the electrolytes. The samples were named PVA-HPO-x, where PVA represents poly(vinyl alcohol), HPO represents H₃PO₄, and x represents the volumetric amount of H₃PO₄ in 20 mL of PVA solution. For instance, PVA-HPO-2 represents the electrolyte containing 2 mL of H₃PO₄ in 20 mL of PVA solution. The precise effects of the water content on the electrolytic properties of the PVA-H₃PO₄ layer are complex and not fully understood in the context of our current research. Further investigation into this aspect, including quantitative measurements of water content and its influence on the sensing characteristics, would provide valuable insights and is an area ripe for future research.

Figure 2a shows the pressure sensitivity at different electrolyte concentrations. It is evident that the sensitivity of the pressure sensor increases with increasing amount of electrolyte. The highest sensitivity was achieved by the PVA-HPO-2 sensor, as shown in Figure 2b, where the sensor achieved a high sensitivity of 2.9 kPa⁻¹ in the 0-16 kPa range and maintained a sensitivity of 1.5 kPa⁻¹ in the 16-90 kPa range. Additionally, the sensor displayed excellent linearity over these broad pressure ranges. This unique performance could be attributed to the synergistic interaction between the electrolyte layer (PVA-H₃PO₄ coated tissue paper) and the porous, conductive carbon cloth electrode. The electrolyte ensures efficient charge storage and transfer, while the carbon cloth's porous structure increases the surface area for electrochemical interaction and provides softness that allows mechanical deformation under pressure.³² These attributes, in conjunction with the supercapacitive sensing technique, create a robust and consistent response, translating physical pressure changes into the corresponding electrical signals with high fidelity and linearity. The pressure sensor demonstrated a broad and almost linear pressure sensing range up to 90 kPa, reflecting the innovative approach taken in this research, leading to precise and repeatable measurements vital for accurate pulse waveform detection (Supplementary Figure S6). The inset of Figure S6 highlights the sensor's ability to detect minute pressures of 6 Pa at the beginning of the pressure sensing, showcasing the sensor's excellent performance. To measure such small pressures, a thick glass slide was placed on the sensor to exert a uniform pressure of 338 Pa. Additional thin and lightweight glass slides were placed on top of the base to create a pressure of approximately 6 Pa on the sensor. Figure 2c shows the sensor's pressure resolution at different pressure loadings, indicating excellent pressure resolution and sufficient discernibility at different pressure loadings of 4, 5, 11, and 16 kPa. The calculated SNR for these pressures demonstrated remarkable values, showcasing the sensor's excellent performance. Specifically, at 4 and 5 kPa pressures, high SNR values of 40.42 and 48.61 dB respectively were

obtained. As the pressure increased to 11 and 16 kPa, the SNR further elevated to 65.38 and 61.31 dB respectively. This enhancement in SNR is attributed to the large-scale signal generation due to the formation of the electrical double layer (EDL) on the electrode-electrolyte interfaces, affirming the superiority of our mechanism in comparison to traditional parallel plate capacitive sensors. The detailed calculation and analysis of the SNR have been provided in the Supporting Information. Furthermore, the sensor exhibited ability in resolving pressure at different low-pressure loadings. Figure 2d illustrates the sensor's ability to resolve pressure in both lowpressure and ultralow-pressure situations. The inset of Figure 2d reveals that the sensor can detect even subtle low-pressure signals (10 Pa) such as those generated by lightweight glass slides. Nevertheless, there is a noticeable shift in the baseline toward higher capacitance during the detection of low and ultralow pressure. This shift may originate from the accumulation of charge due to the electrolytic behavior at each loading cycle. While such accumulation might remain inconspicuous during low-pressure loading, it becomes quite pronounced during ultralow pressure loading, as demonstrated in this specific experiment. The low-pressure resolution is crucial for detecting the intrinsic features from the pulse waveforms while maintaining sufficient SNR. The study found that increasing the electrolytic concentration improved the pressure sensitivity of the sensor but also increased the sensor's hysteresis behavior as shown in Figure 2e,f. The main origin of this undesirable behavior might be the inelastic mechanical deformation of the electrolyte layer. Under pressure, the electrolyte layer experiences mechanical deformation, leading to a lag in its ability to return to its original state once the pressure is removed. This mechanical hysteresis originates from the viscoelastic property of the polymer, affecting the capacitive sensors due to their geometry-dependent sensing mechanism.³³ This mechanical hysteresis might be the primary factor contributing to the observed capacitive hysteresis.³⁴ In addition to mechanical deformation, the electrolytic behavior of the capacitor also plays a role in the hysteresis. Due to the porous structure of the electrode, there might be trapped charge due to irreversible charge transfer leading to hysteresis.³⁵ As the concentration of the electrolyte increases, so does the number of available charge carriers, leading to higher hysteresis at a higher concentration. Figure 2g shows the stability of the pressure sensor when cycled for 5000 times, and the sensor's response time was estimated under loadingunloading of 16 kPa, as shown in Figure 2h. The insets of the cyclic performance show 50 cycles from the beginning (100-150) and 50 cycles from the end (4500-4550) demonstrating similar capacitance retention at the beginning and end of the cycles. The performance decay could be attributed to the hysteresis behavior. The observed loss of capacitance within the initial 100 cycles and the final 100 cycles amounts to a decay of less than 6%. The rise and fall times of the sensor were 0.2 and 0.098 s, respectively, indicating a fast response time for practical applications. Supercapacitive pressure sensors have temperature- and frequency-dependent behaviors as shown in Supplementary Figures S7 and S8 respectively. The capacitance response decreases as the temperature increases (Figure S7). The increase in frequency also decreases the capacitance response, as demonstrated from Figure S8.

The sensor was employed for monitoring cardiovascular activities from different arterial locations. To ensure the comfort of the wearer and consistent measurement, a wrist cuff

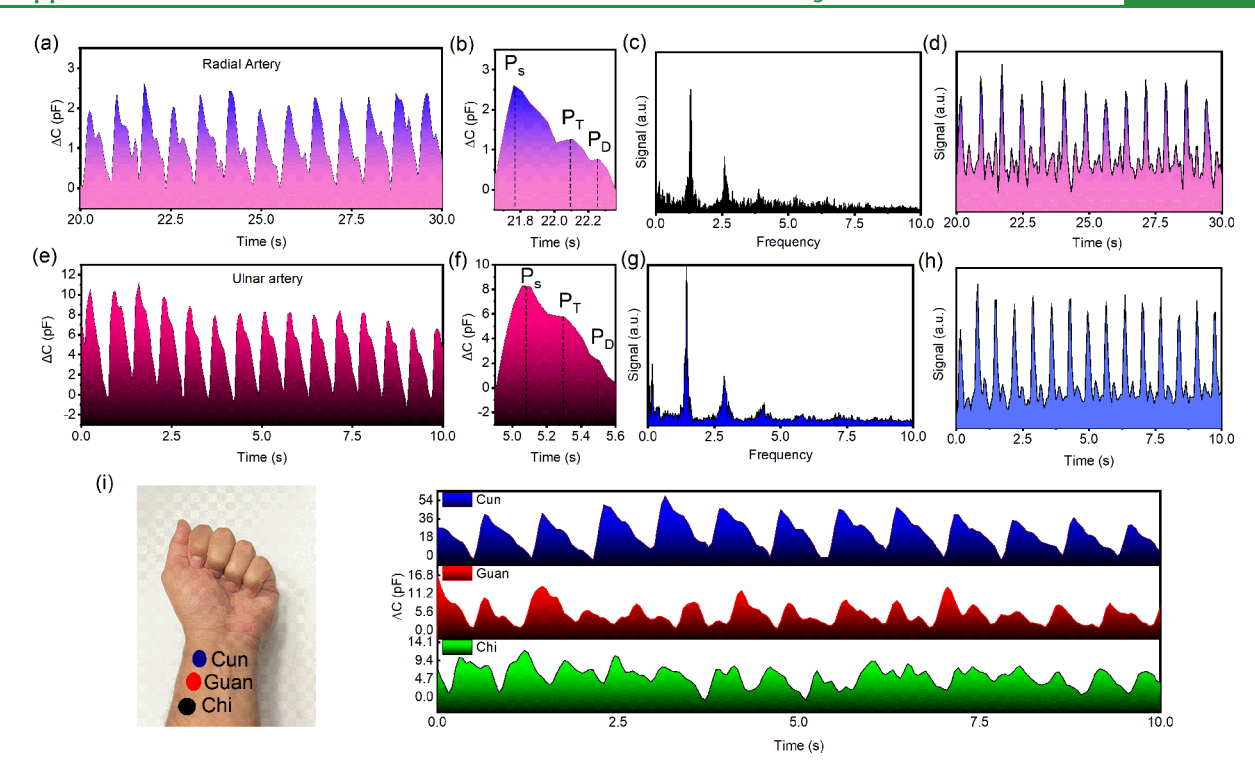


Figure 3. (a) Acquired pulse waveforms from the radial artery. (b) Enlarged view of the pulse waveforms from the radial artery. (c) Fast Fourier transform of the pulse waveforms. (d) First-order derivative of the radial arterial pulse waveforms. (e) Acquired pulse waveforms from the ulnar artery. (f) Enlarged view of the pulse waveforms from the ulnar artery. (g) Fast Fourier transform of the pulse waveforms. (h) First-order derivative of the ulnar arterial pulse waveforms. (i) Pulse waveforms collected from the Cun, Guan, and Chi locations.

was used to hold the sensor in place on the radial arterial site on the wrist (Supplementary Figure S9). This approach provided a uniform pressure on the sensor, facilitating the acquisition of stable and clear pulse waveforms. Figure 3 displays the sensor's sensing performance in acquiring pulse waveforms from various wrist arterial sites. Specifically, Figure 3a presents the collection of pulse waveforms from the radial artery in the wrist, which demonstrates the sensor's capability to obtain uniform pulse waveforms. The uniform pulse waveform collection is attributed to the sensor's high sensitivity, good SNR, excellent pressure resolution, and the precise placement of the sensor using a wrist cuff/band. An enlarged view of the pulse waveforms collected from the radial artery is presented in Figure 3b. The detailed pulse waveform showcases the systolic, diastolic, and inflection peaks, which are characteristic of a regular pulse waveform. Supplementary Movie M1 shows a real-time pulse waveform collection using the fabricated sensor. The early systolic peak (P_S) results from the ventricular contraction, squeezing blood out of the heart, followed by the reflected peak (P_T) . The diastolic peak (P_D) corresponds to the reflection from the lower body.³⁶ The extracted pulse features include the augmentation index (AI_r = P_T/P_S), the digital volume pulse ($\Delta T_{DVP} = T_{PT} - T_{PS}$), the ratio between systolic and diastolic peaks (P_D/P_S), the auxiliary blood pressure index (k), and other derivatives of the above relations. Augmentation index and digital volume pulse are highly related to cardiovascular health. 6,36,37 A healthy and elastic artery exhibits small AI_r and long $\Delta T_{\rm DVP}$. With age, the inflection point and dicrotic notch tend to fade from the pulse waveforms due to the high stiffness and poor elasticity of the blood artery. This leads to a high AI_r and short ΔT_{DVP} for older people. The k value is a convenient assessing index for characterizing an individual's health, which could be

categorized as "low-resistance type" (k < 0.35), "mediumresistance type" (0.35 < k < 0.4), "high-resistance type" (0.4 <k < 0.45), and "ultrahigh-resistance type" (0.45 < k < 0.5). The volunteer's AI_r and ΔT_{DVP} obtained from the radial artery were 0.69 and 175 ms, respectively, indicating a healthy artery. 17 Other pulse waveform characterizations from the radial artery are summarized in Supplementary Table S2. Figure 3c displays the frequency spectrum distribution of the acquired pulse waveforms through the fast Fourier transformation (FFT). Based on the first main peak of the FFT analysis, the pulse rate was calculated to be 80. The first-order differential of the pulse waveforms is essential for further analysis of the pulse waveforms for different applications, such as monitoring the heart rate. The acquired signal was very clean; therefore, the first-order differential showed a very high SNR due to the absence of any unwanted noise (Figure 3d). The first-order differential of the pulse waveforms is also important for calculating pulse transit time for blood pressure monitoring.³⁸ The pulse waveforms were also collected from the ulnar artery in the wrist, as shown in Figure 3e, and demonstrated similar high-quality signal acquisition as the radial arterial pulse waveform collection. The detailed pulse waveform shows all of the characteristics of the pulse waveforms (Figure 3f). Similar to the case for the radial artery, the AI_r of the ulnar artery was found to be 0.7, and $\Delta T_{\rm DVP}$ was found to be 175 ms. Other important characteristics of the pulse waveforms from the ulnar artery are shown in Supplementary Table S2. Finally, Figure 3g displays the ulnar pulse waveform collection showing a frequency of 1.45 Hz, corresponding to 87 BPM. Besides, the first-order differential of the ulnar pulse waveforms shows clean signals indicating high SNR (Figure 3h). The heart rate obtained from both

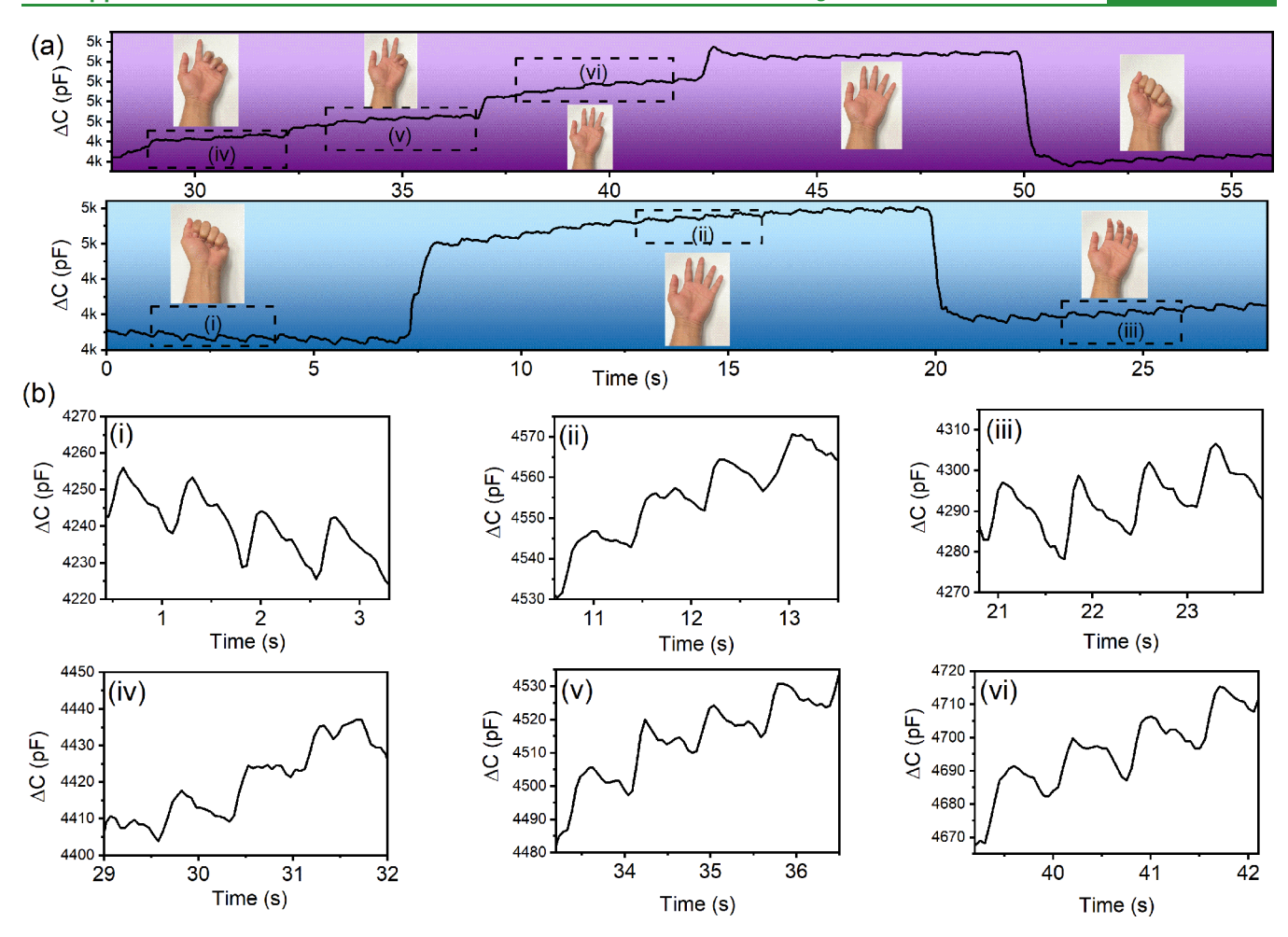


Figure 4. Pulse waveform collection during hand movements. (a) Continuous pulse waveform collection at different hand movements. (b) Detailed view of the pulse waveforms at different hand movements.

radial and ulnar arteries was found to be within the normal range for a healthy person.⁶

Pulse waveforms hold significant importance in traditional Chinese medicine (TCM).³⁶ The TCM practitioner checks the pulse waveforms from the wrist artery for disease diagnosis, specifically examining the pulse shape, strength, and speed at different radial arterial locations designated by Cun, Guan, and Chi as shown in Figure 3i. 37 These locations provide important diagnostic information regarding the heart (left Cun), liver (left Guan), kidney (left and right Chi), lung (right Cun), and spleen (right Guan). ³⁶ To test the sensor's capability, the pulse waveforms were collected from the Cun, Guan, and Chi locations as shown in Figure 3i. The sensor successfully detected the pulse waveforms from different arterial locations. However, the Cun arterial site proved to be the most effective place for pulse waveform collection, since the artery is close to the skin at that location. At the Guan and Chi locations, the artery is further buried under the skin, making it challenging to obtain pulse waveforms with a high SNR. As a result, the pulse waveforms collected from the Guan and Chi have a low SNR.

Figure 4 demonstrates the pressure sensor's sensing performance for pulse waveform acquisition during different hand movements. The sensor effectively discerned the pulse waveforms from the muscular movements of the hand. For instance, Figure 4a-i,b-i illustrate the pulse waveform collection during a closed fist. When the fist is opened and extended, the muscle tensed, and more pressure is put on the pressure

sensor, resulting in a baseline shift of the capacitance (Figure 4a-ii). However, the baseline shift did not affect the quality of the pulse waveforms, as shown in Figure 4b-ii. As the muscle relaxed (Figure 4a-iii), the baseline shifted down again, but the pulse waveform collection remained of good quality, as depicted in Figure 4b-iii. Additionally, Figure 4a-iv-vi displays the muscular movement during different finger movements. Similarly, the acquired pulse waveforms during finger movements shifted the baseline capacitance without significantly altering the pulse waveform's quality (Figure 4b-iv-vi). The pressure sensor's excellent sensing performance can be attributed to its broad and linear pressure sensing range. The pressure sensor has a highly sensitive, linear sensing range, allowing it to detect smaller pulsatile movements from the arteries despite the effects of muscular movements on the pressure sensor.

The sensor was utilized to collect pulse waveforms under varying pressure to investigate the device's performance and shape changes of the pulse waveforms under different pressures. Figure 5a illustrates the sensor's performance under various pressures. During this study, an accurate external pressure was applied to the sensor using a standard cuff-based sphygmomanometer system. The pressure was varied from 20 mmHg (2.66645 kPa) to 110 mmHg (14.6655 kPa), which lies well below the sensor's linear pressure sensing range. As the pressure increases, the pulsatile information from the pulse waveforms becomes clearer since the sensor is being pressed

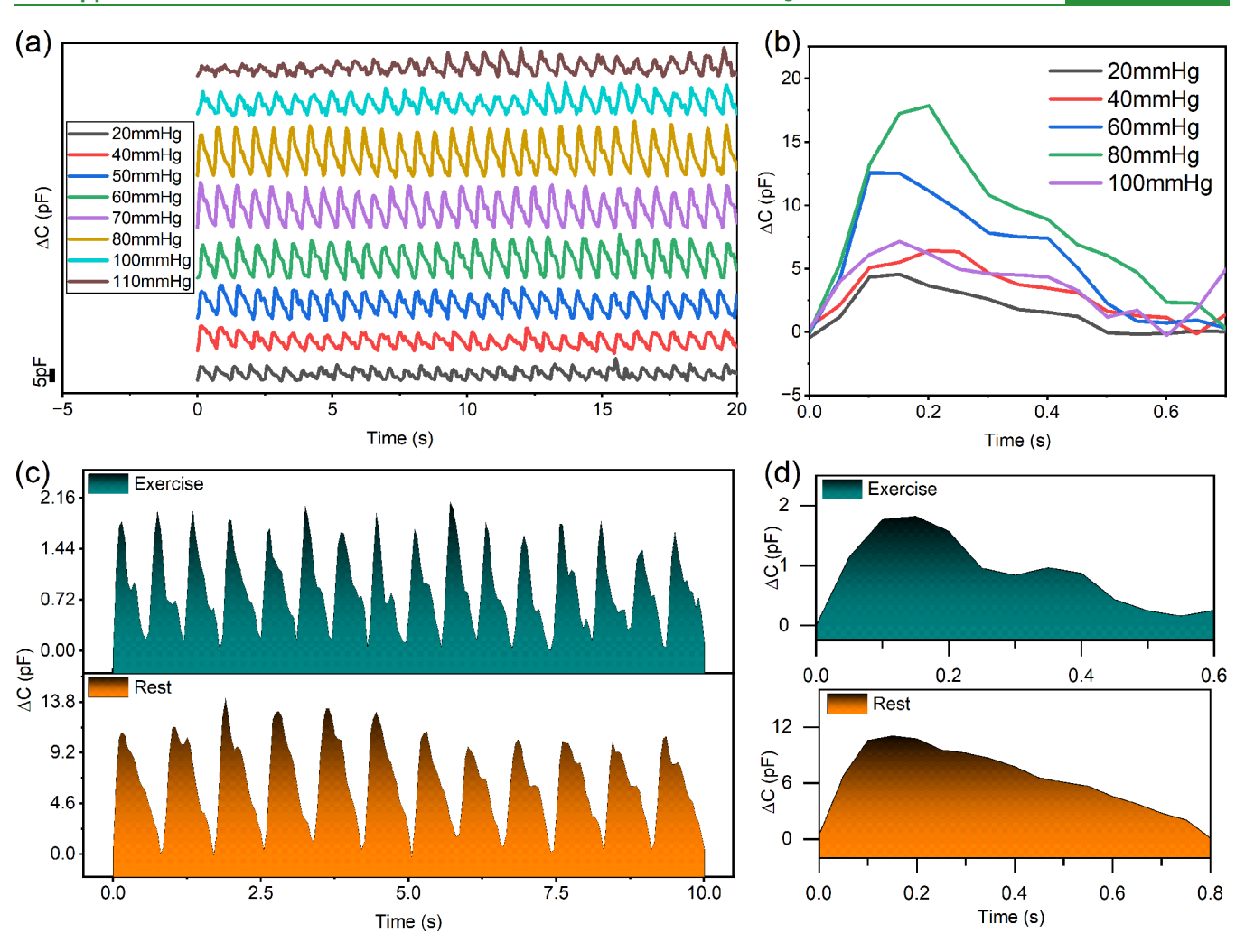


Figure 5. (a) Effects of external pressure on the pulse waveforms. (b) Effects of external pressure on a single pulse waveform. (c) Pulse waveform collection during rest and exercise. (d) Detailed view of the single pulse waveform during rest and exercise.

closer to the artery, resulting in a significant increase in the amplitude of the pulse waveform signal. However, the pulsatile information becomes faded at 80 mmHg, although the amplitude of the pulse waveform signal is the highest under that pressure. Moreover, as the pressure exceeds 80 mmHg (10.6658 kPa), the pulse amplitude starts to decrease (Figure 5b). This occurs due to the increased pressure that partially occludes the blood flow in the artery. With further pressure, the pulse waveform signal becomes unstable and irregular (Figure 5a). This study can be used to determine the optimal external pressure for acquiring high-quality pulse waveforms without harming the wearer. Additionally, the analysis provides crucial cardiovascular information such as pulse velocity, time gap, and intensity ratio (Figure 5b).

To prove the sensor's viability for continuous day-to-day use, pulse waveforms must be acquired during different activities. Figure 5c demonstrates that the sensor can effectively acquire pulse waveforms during rest and exercise, maintaining consistent performance and responsiveness. Figure 5d shows the detailed pulse waveforms during the rest and exercise, respectively. The detailed pulse waveforms indicate that the sensor could detect all intrinsic peaks during rest and exercise. The $\Delta T_{\rm DVP}$ and $\Delta T_{\rm LVP}$ are found to be 150 ms and 0.79 during rest and 100 ms and 0.6 during exercise, respectively. As a valuable application, the sensor was employed to obtain pulse

waveforms from a pregnant woman at 5 and 7 months of pregnancy, as shown in Supplementary Figures S10 and S11, respectively. The acquired pulse waveforms exhibit all characteristic peaks, indicating a healthy pregnancy. The $\Delta T_{\rm DVP}$ and AI_r were found to be 100 ms and 0.815 at 5 months of pregnancy and 75 ms and 0.81 at 7 months of pregnancy, respectively. This trend is consistent with the literature. However, it is important to note that the data for this study were acquired from a single volunteer during mid and late pregnancy, limiting the conclusiveness of the observations. While the observed pattern may suggest that aortic elasticity improves first and then worsens during a normal pregnancy, this finding should be interpreted with caution. Further research involving a more substantial number of volunteers is necessary to validate this indication. Evidently, the ΔT_{DVP} decreases due to an increase in heart rate, and the AI, changes from 0.82 to 0.81. While promising as a potential diagnostic tool, our results underscore the need for broader validation. Further crucial characterizations regarding the pulse waveforms are shown in Supplementary Table S2. In addition to acquiring pulse waveforms from the wrist artery, the sensor could also detect pulse waveforms from the carotid artery, as shown in Supplementary Figure S12. The sensor was placed on top of the carotid artery using a bandage and stable pulse waveforms could be achieved.

4. CONCLUSION

In summary, this study has successfully developed a flexible and highly sensitive supercapacitive pressure sensor through a fast and low-cost fabrication process using tissue paper. The sensor demonstrated excellent sensing capabilities with high cyclability, SNR, and a wide pressure sensing range. The sensor's application has shown potential in detecting arterial pulse waveforms from different arterial locations and performed well during rest and exercise, indicating its potential in wearable health monitoring devices. Additionally, the sensor exhibited a resolution of 10 Pa, which effectively detected pulse waveforms during muscle movements. Its broad and linear pressure sensing range allowed the sensor to detect pulse waveforms before complete arterial occlusion. These applications highlight the great potential of this sensor for commercial use.

ASSOCIATED CONTENT

Supporting Information

The Supporting Information is available free of charge at https://pubs.acs.org/doi/10.1021/acsami.3c08720.

SEM images of the tissue paper, EDS analysis of the PVA–H₃PO₄ impregnated tissue paper, optical image of the sensor, SEM image of the electrode, pressure sensing mechanism, full range of pressure detection, SNR calculation, SNR for different pressure loading, effect of temperature, effect of frequency, sensor placement on the wrist, detailed pulse waveforms at 5 and 7 months of pregnancy, pulse waveforms collected from the carotid artery, characterization of the pulse waveforms (PDF) Real-time pulse waveform monitoring (MP4)

AUTHOR INFORMATION

Corresponding Author

Chunlei Wang — Mechanical and Aerospace Engineering, University of Miami, Coral Gables, Florida 33146, United States; Department of Mechanical and Materials Engineering, Florida International University, Miami, Florida 33174, United States; Email: wangc@miami.edu

Authors

Azmal Huda Chowdhury — Department of Mechanical and Materials Engineering, Florida International University, Miami, Florida 33174, United States; orcid.org/0000-0003-0290-628X

Borzooye Jafarizadeh – Department of Mechanical and Materials Engineering, Florida International University, Miami, Florida 33174, United States

Nezih Pala – Department of Electrical and Computer Engineering, Florida International University, Miami, Florida 33174, United States

Complete contact information is available at: https://pubs.acs.org/10.1021/acsami.3c08720

Funding

This research was funded by National Science Foundation (NSF) Engineering Research Center for Precise Advanced Technologies and Health Systems for Underserved Populations (PATHS-UP ERC) with award #1648451.

Notes

The authors declare no competing financial interest.

Institutional Review Board Statement: On-skin experiments were conducted with the approval from institutional review board (IRB) bearing approval number IRB-20-0079-AM03.

ACKNOWLEDGMENTS

The authors acknowledge the National Science Foundation (NSF) Engineering Research Center for Precise Advanced Technologies and Health Systems for Underserved Populations (PATHS-UP ERC). The authors acknowledge the partial support from the NSF awards #2126190, #2301898, and #2107318. Additionally, A.C. and B.J. acknowledge the Dissertation Year Fellowship (DYF) and Doctoral Evidence Acquisition Fellowship (DEA) respectively from Florida International University graduate school. The authors greatly acknowledge the discussions from Dr. Jessica Ramella-Roman at Florida International University and Dr. Gerard L. Coté from Texas A&M University. The authors would like to acknowledge Center for Study of Matter at Extreme Conditions (CESMEC) at Florida International University.

REFERENCES

- (1) Mishra, S.; Mohanty, S.; Ramadoss, A. Functionality of Flexible Pressure Sensors in Cardiovascular Health Monitoring: A Review. ACS Sensors 2022, 7 (9), 2495–2520.
- (2) Zhang, Q.; Shen, L.; Liu, P.; Xia, P.; Li, J.; Feng, H.; Liu, C.; Xing, K.; Song, A.; Li, M.; et al. Highly sensitive resistance-type flexible pressure sensor for cuffless blood-pressure monitoring by using neural network techniques. *Composites Part B: Engineering* **2021**, 226, 109365.
- (3) Luo, N.; Dai, W.; Li, C.; Zhou, Z.; Lu, L.; Poon, C. C. Y.; Chen, S.-C.; Zhang, Y.; Zhao, N. Flexible Piezoresistive Sensor Patch Enabling Ultralow Power Cuffless Blood Pressure Measurement. *Adv. Funct. Mater.* **2016**, *26* (8), 1178–1187.
- (4) Chowdhury, A. H.; Jafarizadeh, B.; Pala, N.; Wang, C. Wearable Capacitive Pressure Sensor for Contact and Non-Contact Sensing and Pulse Waveform Monitoring. *Molecules* **2022**, *27*, 6872.
- (5) Boutry, C. M.; Nguyen, A.; Lawal, Q. O.; Chortos, A.; Rondeau-Gagné, S.; Bao, Z. A Sensitive and Biodegradable Pressure Sensor Array for Cardiovascular Monitoring. *Adv. Mater.* **2015**, *27* (43), 6954–6961.
- (6) Yang, T.; Jiang, X.; Zhong, Y.; Zhao, X.; Lin, S.; Li, J.; Li, X.; Xu, J.; Li, Z.; Zhu, H. A Wearable and Highly Sensitive Graphene Strain Sensor for Precise Home-Based Pulse Wave Monitoring. *ACS Sensors* **2017**, 2 (7), 967–974.
- (7) Meng, K.; Xiao, X.; Wei, W.; Chen, G.; Nashalian, A.; Shen, S.; Xiao, X.; Chen, J. Wearable Pressure Sensors for Pulse Wave Monitoring. *Advanced Materials* **2022**, *34*, 2109357.
- (8) Pan, L.; Han, L.; Liu, H.; Zhao, J.; Dong, Y.; Wang, X. Flexible sensor based on Hair-like microstructured ionic hydrogel with high sensitivity for pulse wave detection. *Chem. Eng. J.* **2022**, *450*, 137929.
- (9) Li, J.; Bao, R.; Tao, J.; Peng, Y.; Pan, C. Recent progress in flexible pressure sensor arrays: from design to applications. *Journal of Materials Chemistry C* **2018**, 6 (44), 11878–11892.
- (10) Jafarizadeh, B.; Chowdhury, A. H.; Khakpour, I.; Pala, N.; Wang, C. Design Rules for a Wearable Micro-Fabricated Piezo-Resistive Pressure Sensor. *Micromachines* **2022**, *13* (6), 838.
- (11) Yoon, S. G.; Park, B. J.; Chang, S. T. Highly Sensitive Piezocapacitive Sensor for Detecting Static and Dynamic Pressure Using Ion-Gel Thin Films and Conductive Elastomeric Composites. ACS Appl. Mater. Interfaces 2017, 9 (41), 36206–36219.
- (12) Mahata, C.; Algadi, H.; Lee, J.; Kim, S.; Lee, T. Biomimetic-inspired micro-nano hierarchical structures for capacitive pressure sensor applications. *Measurement* **2020**, *151*, 107095.
- (13) Thouti, E.; Nagaraju, A.; Chandran, A.; Prakash, P. V. B. S. S.; Shivanarayanamurthy, P.; Lal, B.; Kumar, P.; Kothari, P.; Panwar, D. Tunable flexible capacitive pressure sensors using arrangement of

- polydimethylsiloxane micro-pyramids for bio-signal monitoring. Sens. Actuators, A 2020, 314, 112251.
- (14) Zhao, S.; Ran, W.; Wang, D.; Yin, R.; Yan, Y.; Jiang, K.; Lou, Z.; Shen, G. 3D Dielectric Layer Enabled Highly Sensitive Capacitive Pressure Sensors for Wearable Electronics. ACS Appl. Mater. Interfaces **2020**, 12 (28), 32023-32030.
- (15) Cho, S. H.; Lee, S. W.; Yu, S.; Kim, H.; Chang, S.; Kang, D.; Hwang, I.; Kang, H. S.; Jeong, B.; Kim, E. H.; et al. Micropatterned Pyramidal Ionic Gels for Sensing Broad-Range Pressures with High Sensitivity. ACS Appl. Mater. Interfaces 2017, 9 (11), 10128-10135.
- (16) Choi, J.; Kwon, D.; Kim, K.; Park, J.; Orbe, D. D.; Gu, J.; Ahn, J.; Cho, I.; Jeong, Y.; Oh, Y.; et al. Synergetic Effect of Porous Elastomer and Percolation of Carbon Nanotube Filler toward High Performance Capacitive Pressure Sensors. ACS Appl. Mater. Interfaces 2020, 12 (1), 1698-1706.
- (17) Mu, C.; Li, J.; Song, Y.; Huang, W.; Ran, A.; Deng, K.; Huang, J.; Xie, W.; Sun, R.; Zhang, H. Enhanced Piezocapacitive Effect in CaCu3Ti4O12-Polydimethylsiloxane Composited Sponge for Ultrasensitive Flexible Capacitive Sensor. ACS Applied Nano Materials **2018**, 1 (1), 274–283.
- (18) Qiu, Z.; Wan, Y.; Zhou, W.; Yang, J.; Yang, J.; Huang, J.; Zhang, J.; Liu, Q.; Huang, S.; Bai, N.; et al. Ionic Skin with Biomimetic Dielectric Layer Templated from Calathea Zebrine Leaf. Adv. Funct. Mater. 2018, 28 (37), 1802343.
- (19) Henriques, A.; Rabiei Baboukani, A.; Jafarizadeh, B.; Chowdhury, A. H.; Wang, C. Nano-Confined Tin Oxide in Carbon Nanotube Electrodes via Electrostatic Spray Deposition for Lithium-Ion Batteries. Materials 2022, 15, 9086.
- (20) Banerjee, R.; Chowdhury, A. H.; Kumar, P. S.; Wang, C.; Goel, S.; Raj, P. M. Laser-induced graphene supercapacitors on flex substrates for package-integrated power supply. 2023 Fourth International Symposium on 3D Power Electronics Integration and Manufacturing (3D-PEIM) 2023, 1-5.
- (21) Sharma, S.; Chhetry, A.; Sharifuzzaman, M.; Yoon, H.; Park, J. Y. Wearable Capacitive Pressure Sensor Based on MXene Composite Nanofibrous Scaffolds for Reliable Human Physiological Signal Acquisition. ACS Appl. Mater. Interfaces 2020, 12 (19), 22212-22224.
- (22) Zhou, H.; Wang, M.; Jin, X.; Liu, H.; Lai, J.; Du, H.; Chen, W.; Ma, A. Capacitive Pressure Sensors Containing Reliefs on Solution-Processable Hydrogel Electrodes. ACS Appl. Mater. Interfaces 2021, 13 (1), 1441-1451.
- (23) Chowdhury, A. H.; Khakpour, I.; Jafarizadeh, B.; Pala, N.; Wang, C. A Facile Fabrication of Porous and Breathable Dielectric Film for Capacitive Pressure Sensor. 2020 IEEE SENSORS 2020, 1-
- (24) Sun, G.; Wang, P.; Jiang, Y.; Sun, H.; Meng, C. Intrinsically Flexible and Breathable Supercapacitive Pressure Sensor Based on MXene and Ionic Gel Decorating Textiles for Comfortable and Ultrasensitive Wearable Healthcare Monitoring. ACS Applied Electronic Materials 2022, 4 (4), 1958-1967.
- (25) Nie, B.; Li, R.; Cao, J.; Brandt, J. D.; Pan, T. Flexible Transparent Iontronic Film for Interfacial Capacitive Pressure Sensing. Advanced Materials 2015, 27, 6055.
- (26) Li, R.; Si, Y.; Zhu, Z.; Guo, Y.; Zhang, Y.; Pan, N.; Sun, G.; Pan, T. Supercapacitive Iontronic Nanofabric Sensing. Adv. Mater. 2017, 29 (36), 1700253.
- (27) Chhetry, A.; Kim, J.; Yoon, H.; Park, J. Y. Ultrasensitive Interfacial Capacitive Pressure Sensor Based on a Randomly Distributed Microstructured Iontronic Film for Wearable Applications. ACS Appl. Mater. Interfaces 2019, 11 (3), 3438-3449.
- (28) Sharma, S.; Chhetry, A.; Zhang, S.; Yoon, H.; Park, C.; Kim, H.; Sharifuzzaman, M.; Hui, X.; Park, J. Y. Hydrogen-Bond-Triggered Hybrid Nanofibrous Membrane-Based Wearable Pressure Sensor with Ultrahigh Sensitivity over a Broad Pressure Range. ACS Nano 2021, 15 (3), 4380-4393.
- (29) Bai, N.; Wang, L.; Wang, Q.; Deng, J.; Wang, Y.; Lu, P.; Huang, J.; Li, G.; Zhang, Y.; Yang, J.; et al. Graded intrafillable architecturebased iontronic pressure sensor with ultra-broad-range high sensitivity. Nat. Commun. 2020, 11 (1), 209.

- (30) Alipoori, S.; Torkzadeh, M. M.; Mazinani, S.; Aboutalebi, S. H.; Sharif, F. Performance-tuning of PVA-based gel electrolytes by acid/ PVA ratio and PVA molecular weight. SN Applied Sciences 2021, 3 (3), 310.
- (31) Mansur, H. S.; Sadahira, C. M.; Souza, A. N.; Mansur, A. A. P. FTIR spectroscopy characterization of poly (vinyl alcohol) hydrogel with different hydrolysis degree and chemically crosslinked with glutaraldehyde. Materials Science and Engineering: C 2008, 28 (4),
- (32) Zhong, Y.; Gu, F.; Wu, L.; Wang, J.; Dai, S.; Zhu, H.; Cheng, G.; Ding, J. Porous conductive electrode for highly sensitive flexible capacitive pressure sensor over a wide range. J. Alloys Compd. 2023, 934, 167919.
- (33) Hwang, J.; Lee, S. G.; Kim, S.; Kim, J. S.; Kim, D. H.; Lee, W. H. Unveiling Viscoelastic Response of Capacitive-type Pressure Sensor by Controlling Cross-Linking Density and Surface Structure of Elastomer. ACS Applied Polymer Materials 2020, 2 (6), 2190-2198.
- (34) Ruth, S. R. A.; Bao, Z. Designing Tunable Capacitive Pressure Sensors Based on Material Properties and Microstructure Geometry. ACS Appl. Mater. Interfaces 2020, 12 (52), 58301-58316.
- (35) Gupta, S.; Price, C. Investigating graphene/conducting polymer hybrid layered composites as pseudocapacitors: Interplay of heterogeneous electron transfer, electric double layers and mechanical stability. Composites, Part B 2016, 105, 46-59.
- (36) Wang, J.; Zhu, Y.; Wu, Z.; Zhang, Y.; Lin, J.; Chen, T.; Liu, H.; Wang, F.; Sun, L. Sun, L. Wearable multichannel pulse condition monitoring system based on flexible pressure sensor arrays. Microsyst. Nanoeng. 2022, 8 (1), 16.
- (37) Lin, Q.; Huang, J.; Yang, J.; Huang, Y.; Zhang, Y.; Wang, Y.; Zhang, J.; Wang, Y.; Yuan, L.; Cai, M.; et al. Highly Sensitive Flexible Iontronic Pressure Sensor for Fingertip Pulse Monitoring. Adv. Healthcare Mater. 2020, 9 (17), 2001023.
- (38) Jin, Y.; Chen, G.; Lao, K.; Li, S.; Lu, Y.; Gan, Y.; Li, Z.; Hu, J.; Huang, J.; Wen, J. dentifying human body states by using a flexible integrated sensor. npj Flexible Electron. 2020, 4 (1), 28.